

Numerical Investigation on the Effects of Internal Flow Structure on Ejector Performance

M. Falsafioon[†], Z. Aidoun and K. Ameer

Canmet ENERGY, Natural Resources Canada, 1615 Lionel-Boulet Blvd., Varennes, Quebec, J3X 1S6, Canada

[†] *Corresponding Author Email: mehdi.falsafioon@canada.ca*

(Received December 6, 2018; accepted March 10, 2019)

ABSTRACT

Recent work on ejector performance enhancement indicates that more information on ejector internal flow structure is needed to have a clearer picture of factors and conditions affecting operation and performance of these devices. This paper relies on experimental studies and CFD simulations to identify flow structures occurring under typical ejector refrigeration conditions and primary nozzle geometry and position. Effects on parameter distributions and the resulting operation of the device are given particular attention. The CFD model used for this purpose was validated by using in-house data, generated from an experimental prototype and over a wide range of conditions. The experiments for the selected condition were predicted very satisfactorily by numerical model. The study then focused on the role of the primary nozzle geometry and the distance of the nozzle from the beginning of the mixing chamber (NXP), in locally shaping the flow structure and the related consequences on ejector operation. Simulations on NXP for given operating conditions have shown that an optimum value was always found, and slightly varied the operating conditions within the range considered. Primary nozzle shape changes in terms of outlet diameters for given upstream conditions directly affected the expansion level of the flow. The simulations showed that an optimum range of nozzle exit diameters could be found, for which ejector performance was highest. Moreover, under these conditions it was observed that pressure fluctuations inside the ejector were reduced.

Keywords: Ejector performance; Ejector configuration; CFD simulation; Performance improvement.

1. INTRODUCTION

A fixed geometry ejector works efficiently only in a very narrow range around its design point. However, in off-design conditions, its performance degrades rapidly. Ejector performance is very sensitive to operating conditions and the influence of a number of its geometrical features, to various extents. The factors mostly known to be relevant are the nozzle exit position (NXP) and the mixing chamber diameter (D_{mix}), but parameters such as the nozzle exit diameter (D_{pnx}) and the mixing chamber length ratio (L_{mix}/D_{mix}) do influence performance as well. These have been studied numerically and experimentally at various degrees of detail by many researchers, typically (Aphornratana and Eames 1997), (Chunnanond and Aphornratana; 2004), (Boumaraf and Lallemand 2005), (Yapıcı; 2008), (Varga, Oliveira, and Diaconu; 2009), (Chong, Hu, Chen, Wang, Liu, and Yan; 2014), to name only a few. The NXP parameter indicates the positioning of the primary nozzle (Fig. 1) with respect to the mixing chamber. It is generally defined as the distance from the exit plane of the primary nozzle to the entry plane of the converging entrance zone of the mixing chamber (Nahdi, Champoussin, Hostache, and Cheron; 1993). In some cases, others (e.g. Huang,

Chang, Wang, and Petrenko; 1999) consider the positioning of the primary nozzle relative to the inlet of the mixing chamber throat, especially in the case of constant area ejectors. Varying NXP by axially moving the nozzle forward or backward in the mixing chamber affects ejector performance. This parameter is sometimes presented in its non-dimensional form as NXP/D_{mix} (Eames, Wu, Worall, and Aphornratana, 1999). For example, Riffat *et al.* (Riffat and Omer; 2001) selected four NXP locations (two negative, one at inlet and one inside the mixing chamber) for an ejector operating with methanol. Maximum entrainment ratio was found to occur for a location outside the mixing chamber for the chosen conditions, in agreement with ESDU recommendations. In contrast, Rusly *et al.* (Rusly, Aye, Charters, and Ooi, 2005) did not observe any important change of performance within the range of $\pm 20\%$ NXP variation of their ejector design. Pianthong *et al.*'s (Pianthong, Seehanam, Behnia, Sriveerakul, and Aphornratana; 2007) CFD analysis of a steam ejector confirmed the NXP effect on the performance, and observed that for given operating conditions, only one value corresponded to optimal operation. Similar results were obtained experimentally by (Pianthong, Seehanam, Behnia, Sriveerakul, and Aphornratana; 2007) with R245fa

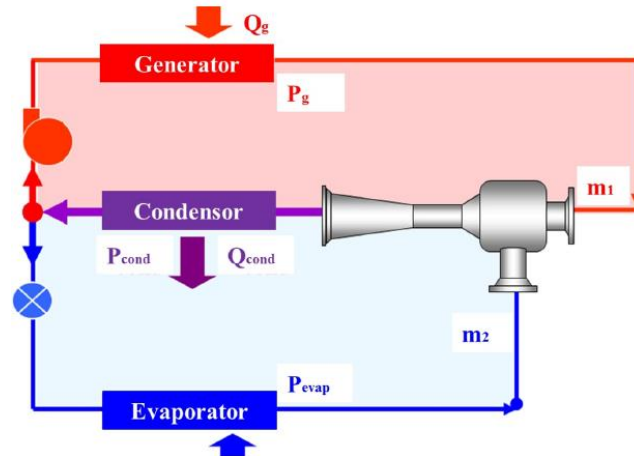
on a CRMC type jet pump. Varga *et al.* (Varga, Oliveira, and Diaconu, 2009) reported that the optimal value of NXP coincided with the maximal value of critical back pressure. Chen *et al.* (Chen, Chong, Yan, and Liu; 2013) studied numerically the effect of both the NXP and the length of the mixing chamber throat in a non-dimensional form for a case of natural gas application. Unlike (Varga, Oliveira, and Diaconu, 2009), their findings indicated that NXP presents a different optimum for the entrainment and compression ratios and greatly depended on working primary pressures. Several more simulation and experimental works are worth mentioning in this respect (Sriveerakul, Aphornratana, and Chunnanond 2007b), (Zhu, Cai, Wen, and Li ;2009), (Lin, Cai, Li, Yan, Hu, and Giridharan; 2013), (Yan, Lin, Cai, Chen, and Wang; 2016). They reported optimal ejector operation in terms of NXP for entrainment and compression ratios with several refrigerants, different locations in the mixing chamber and various degrees of performance improvements. There is a fair consensus among all these findings regarding the existence of a value of NXP corresponding to optimal ejector operation, even though more effort is needed to clarify issues like specific effects of the fluid and conditions of operation on both entrainment and compression ratios. This has been tried to be covered in the current study. Also, the effect of NXP remains very dependent on the fluid type, geometry and operating conditions and can only be adjusted on a case-by-case basis. This is also discussed in the current manuscript.

Another important geometrical aspect of an ejector is the primary nozzle shape which is studied in the literature widely. For instance, theoretical, CFD-based assessments of steam ejector were performed by (Ariafar, 2012) and (Ruangtrakoon, Thongtip, Aphornratana, and Sriveerakul; 2013) respectively, in which they compared three nozzles differing only by their outlet diameter, but submitted to the same operating conditions in order to maintain the same primary mass flow rate. It was found that all nozzles achieved the same entrainment ratio ω , while the back pressure increased with the Mach number M_x at the nozzle outlet. Lin *et al.* (Lin, Cai, Li, Yan, Hu, and Giridharan; 2013) numerically performed similar work with a natural gas ejector by varying the nozzle divergent angle, β . They presented the results in terms of nozzle divergent angle for a fixed secondary mass flow rate and a range of primary throat openings (100% to 50%) by means of a spindle. For full open throat, back pressure increased monotonically with β . As the throat was increasingly restricted, an optimal angle value corresponding to maximum back pressure was identified. This implies that for full throat operation, ω remains constant while the back pressure improves, similarly to (Ruangtrakoon, Thongtip, Aphornratana, and Sriveerakul; 2013) findings. With increasing throat restriction, optimal ω steadily increased with a lower rate of increase in the back pressure. The authors attributed the displacement of the optimal angle to the change of the flow inside the nozzle and the critical throat area. This may have as well impacted the importance of the back pressure. Yan *et al.* (Yan,

Cai, Lin, Li, and Li, 2016) conducted experiments with different angles of the primary divergent while maintaining the back pressure constant. The results indicated a maximum variation in the entrainment ratio of 9% when varying the angle in the range of 3.9 to 9.1 degrees. In a recent paper, Thongtip *et al.* (Thongtip and Aphornratana; 2017) continued this work experimentally. They fixed the primary mass flow rate and varied the Mach number M_x at the nozzle outlet by changing the cross section area, while all the other conditions were maintained constant. The result was that ω moderately improved, while the back pressure increased with higher M_x . According to the authors, this may be due to better suction created by higher primary stream velocity, in such a way that the ejector had a stronger drawing potential of the secondary stream and the expansion wave angle being potentially reduced by the lower outlet nozzle pressure, thus resulting in an increase of the effective area for the secondary fluid. The authors pointed out, however, that with a fixed primary flow, there may be a limitation of the heat source in order to produce the design condition for high M_x besides the larger outlet diameter, which may restrict the mixing chamber operation. These works highlighted the importance of geometrical parameters on the performance of an ejector, yet showed contradictory findings regarding their optimal value. The current study tries to represent a more detailed, accurate representation of fluid flow pattern inside ejectors along with changes of two important geometrical aspects and their effects on ejector performance.

2. EJECTOR THEORY

A gas/gas supersonic ejector system may be heat activated to produce a cooling system. Compared to a conventional mechanical compression cycle, in an ejector cycle, the compressor is replaced by the trio pump-generator-ejector. Integrating the ejector in a conventional refrigeration system in order to boost its performance or, in other cases, simply replacing a compressor with a circulation pump and a generator, offers the opportunity to reduce the overall system electricity consumption. Ejector operation consists in using a high primary energy stream mass flow rate (m_1) and expanding it in a supersonic nozzle to entrain and exchange energy with a secondary stream mass flow rate (m_2). This set-up acts like a compressor and can be implemented in a cooling system. The performance is qualified by the entrainment ratio of the secondary to the primary streams ($\omega = m_2/m_1$), and the compression ratio of the outlet pressure to secondary pressure ($p_r = P_{cond}/P_2$). A thermal jump, identified as the "lift", can also be defined as a difference between the condensation temperature (T_{cond}) or the saturated temperature corresponding to the condensation pressure, and the evaporation temperature (T_{evap}) or the saturated temperature corresponding to the evaporation pressure (thermal jump = lift = $T_{cond} - T_{evap}$). The lift characterizes the quality of the cold produced by the ejector.



(a) A schematic of the experimental set up



(b) View of the constructed set-up for the experiments

Fig. 1. Experimental set up.

3. EXPERIMENTAL SETUP

A simplified diagram of the designed prototype is shown in Fig. 1(a). It shows the main components: ejector, generator, evaporator, condenser and refrigerant pump. A view of the constructed prototype is given in Fig. 1(b).

The prototype includes several main components:

- A generator, which is a heat exchanger used to vaporize the high pressure liquid refrigerant;
- A re-generator, which recovers part of the sensible energy of the outgoing gaseous refrigerant from the ejector to preheat the liquid refrigerant to the generator;
- A superheater, which allows more flexibility for adjusting the refrigerant superheat temperature

before its arrival into the ejector;

- A boiler fueled by natural gas, provides steam at 113°C as an energy source for the generator and the super-heater;
- A fluid cooler and its pump, which use a glycol water loop to reject the condensation energy of refrigerant;
- A tank recovering the liquid refrigerant at the condenser outlet;
- An expansion valve used to adjust the pressure of the secondary flow

The prototype consists of three loops; (I) a loop of ejector cycle in a low-pressure part; (II) a loop bringing heat from boiler to the generator and the super-heater; And (III) a loop used for heat rejection to the condenser. An ejector initially installed on the

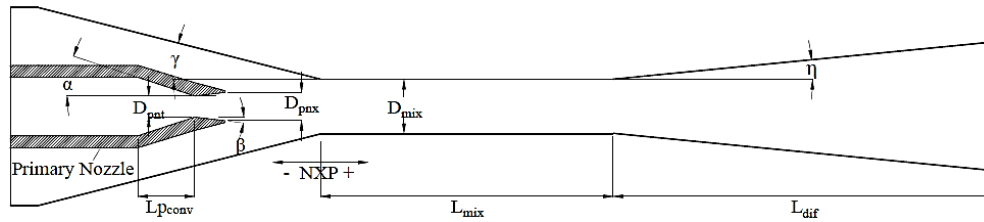


Fig. 2. A schematic of an ejector including geometrical parameters.

Table 1 Correlation matrix showing correlation coefficients between different geometrical parameters

Variable	α	β	γ	L_{pconv}	NXP	D_{PNX}	L_{mix}	D_{mix}	D_{PNT}	ω
α	1	0.81	0.52	0.56	0.77	0.51	0.75	0.63	0.66	0.1
β	0.81	1	0.74	0.76	0.91	0.78	0.69	0.68	0.76	-0.14
γ	0.52	0.74	1	0.99	0.79	0.76	0.34	0.34	0.41	-0.14
L_{pconv}	0.56	0.76	0.99	1	0.8	0.78	0.37	0.37	0.43	-0.14
NXP	0.77	0.91	0.79	0.8	1	0.85	0.64	0.65	0.82	-0.24
D_{PNX}	0.51	0.78	0.76	0.78	0.85	1	0.61	0.7	0.77	-0.65
L_{mix}	0.75	0.69	0.34	0.37	0.64	0.61	1	0.89	0.79	-0.24
D_{mix}	0.63	0.68	0.34	0.37	0.65	0.7	0.89	1	0.86	-0.51
D_{PNT}	0.66	0.76	0.41	0.43	0.82	0.77	0.79	0.86	1	-0.45
ω	0.1	-0.14	-0.14	-0.14	-0.24	-0.65	-0.24	-0.51	-0.45	1

Table 2 Ejector Dimensions

α	β	γ	η	D_{pnt}	D_{pnx}	D_{mix}	NXP	L_{pconv}	L_{dif}	L_{mix}
18°	7°	14°	3°	7.09mm	various	16.4mm	various	17.2mm	250mm	89mm

prototype was designed to work under different operating conditions in order to study the improvement of entrainment ratio.

4. NUMERICAL MODELLING

The performance of an ejector depends on different geometrical parameters (Fig. 2). Different type of ejectors were installed on the experimental set-up in order to evaluate the effect of these geometrical parameters on the ejector performance. Afterwards, close to 5000 experimental data points were used to compose a correlation matrix that shows the correlation between each geometrical parameter and the ejector entrainment ratio (Table 1). This allows to determine those geometrical parameters that have highest correlation with entrainment ratio. Consequently, there are a few that have stronger impacts on the entrainment ratio. These are: 1- The nozzle throat diameter (D_{pnt}) (correlation which is a key element of a nozzle determining the mass flow rate for a certain working condition. However, the nozzle throat by itself does not have any effect on the performance of an ejector and is designed independently of other geometrical parameters. 2- The nozzle exit diameter (D_{pnx}) that has a big impact on the pressure of motive flow exiting the nozzle. 3- The distance between the nozzle exit and the constant area of mixing chamber (NXP). 4- The diameter of the mixing chamber (D_{mix}) and finally 5- The length of mixing chamber (L_{mix}). An in-house designed ejector is modelled in 2-D and is assumed to be axi-symmetric along the x-axis. The previous 3D numerical simulations show that there is no significant 3D effect on ejector performance (e.g.

([Sriveerakul, Aphornratana, and Chunnanond 2007a](#)). An unsteady approach was first considered for the simulations; however, all the results show a convergence to steady-state solutions. Therefore, the conservation equations of continuity, momentum and energy are used in their compressible and steady state forms. Non-linear sets of discretized equations are solved using the commercial software ANSYS Fluent v.18 for a single-phase supersonic ejector with R134a as the working fluid.

4.1 Geometry

The chosen geometry is based on an in-house ejector design which is working on an experimental workbench. Table 2 shows the dimension of the ejector installed on the experimental prototype based on the parameters defined in Fig. 2. A series of comprehensive experiments have been carried out with this supersonic ejector for different working conditions. The experimental results show that the selected ejector works properly for a wide range of working conditions ([Falsafioon, Aidoun, and Poirier; 2017](#)). Because of the limitations of the experimental set-up, all the geometrical parameters are kept fixed during the experiments. CFD model is validated using generated experimental data.

4.2 CFD Model

In compressible flows, the pressure is a function of both density and temperature. Since we are dealing with a high-speed compressible phenomena in-side the ejector, in order to have a better accuracy and resolution of shocks, the system of algebraic equations is solved using a density-based algorithm.

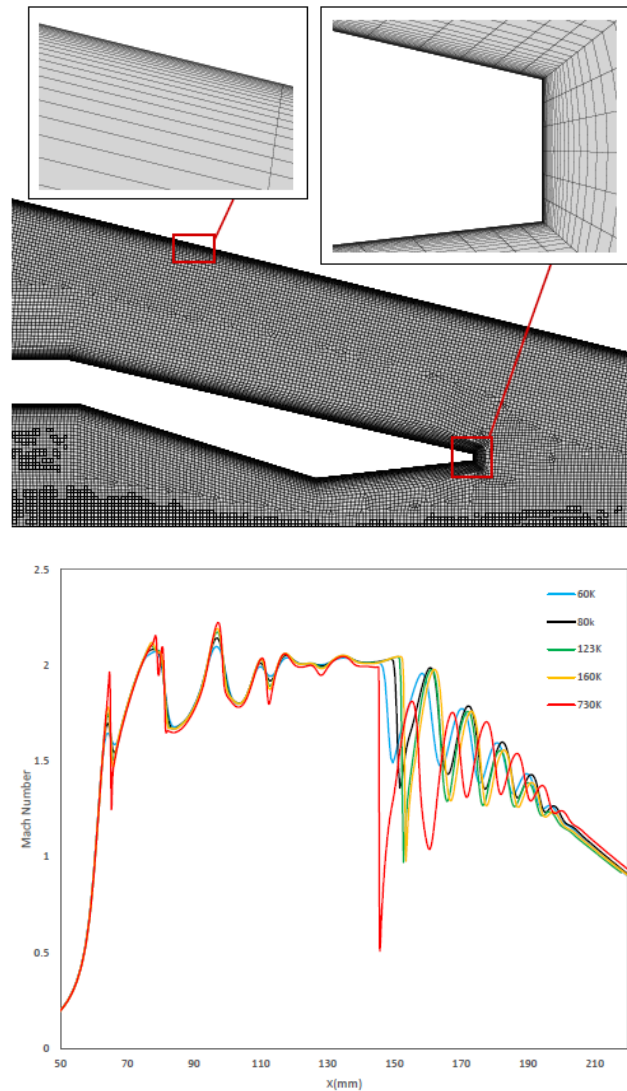


Fig. 3. (a) Generated grid for the CFD model (b) Mach profile along ejector axisymmetry axis in different grid sizes.

However, one may use a pressure-based algorithm which is a trade-off between accuracy and the cost of calculations (Croquer, Poncet, and Aidoun; 2016). NIST real gas model (REFPROP v9.2 database (Lemmon, Huber, and McLinden; 2002) for R134a is used to compute fluid thermodynamic and transport properties. As the main objective of the current work is to investigate the ejector internal flow structure, simulations have been carried out with $k - \epsilon$ and $k - \omega$ SST turbulence models. The $k - \epsilon$ turbulence model is robust and convergence is relatively fast, however presents some weaknesses to calculate near wall flow properties and to predict flow separation. The two equation turbulence model $k - \omega$ SST (Menter, 1994), is well known for its ability to properly model near-wall flow field and is used in the current study. This turbulence model has been tested and validated for ejector studies in the literature (Croquer, Poncet, and Aidoun; 2016; Wang, Yan, Wang, and Li; 2017; Watanawanavet; 2008; Bartosiewicz, Aidoun, Desevaux, and Mercadier 2005). Since $k - \omega$ SST turbulence model

is used, the value of y^+ is kept below 1 ($y^+ \leq 1$) by refining the near wall mesh. A "pressure inlet" boundary condition is applied for both primary and secondary inlets and a "pressure outlet" boundary condition is imposed at the outlet. All walls are considered to be adiabatic with no-slip boundary condition.

4.3 Grid Validation

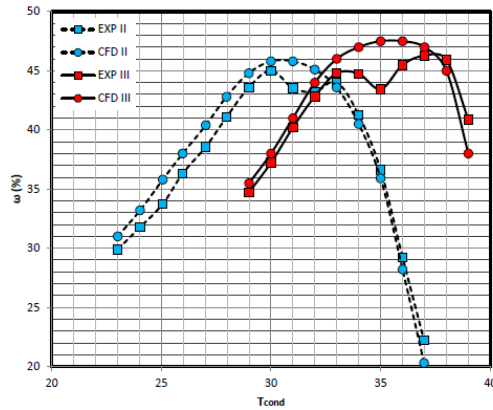
The computational domain is discretized using a tetra dominant mesh generated in ANSYS meshing v.18 for fluid mechanics applications. Global mesh refinement is implemented to test the effect of different grid sizes on CFD model results. Local mesh sizing and grid concentration are also applied at specific locations (sharp corners, curvatures, grid concentration, etc.) in order to have more control on the element size in different locations of the geometry (Fig. 3(a)). These are considered to have better boundary layer resolution and near-wall treatment. Consequently, local and global solution

Table 3 Working conditions for experimental and numerical studies

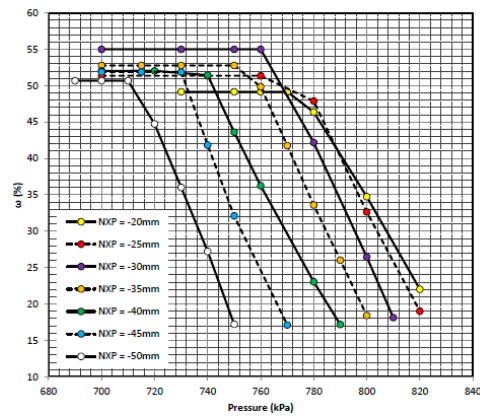
Condition	P_{gen}	T_{gen}	P_{evap}	T_{evap}	$P_{cond(sat)}$
I	2748	97	450	21	various
II	2633	100	425	25	various
III	2900	106	265	50	various

Table 4 Number of elements and corresponding entrainment ratios

Grid Size (number of elements)	60×10^3	80×10^3	123×10^3	160×10^3	730×10^3
Entrainment Ratio (ω)	54.46%	55.01%	55.33%	55.46%	55.80%



a



b

Fig. 4. (a) Entrainment ratio versus ejector exit temperature in saturated state and for a lift of 20°C (b) Entrainment ratio versus ejector outlet pressure for different NXPs.

grid independence criteria were employed to find the size of the grid for which the solution is invariant with finer meshes. To assess the solution grid independence locally, the Mach number profile for operating condition number 2 (Table 3) is drawn along the x-axis (the ejector axisymmetry axis) for different grid sizes. As shown in Fig. 3(b), for a very fine grid size with almost 730×10^3 elements, the locations of shocks happening in mixing chamber is slightly changed which most probably is a better representation of shock positions. However, since this makes the calculations much more expensive, the rest of simulations are carried out using a grid with almost 160×10^3 elements. On the other side, a global solution grid independence check shows that there is no big variation of entrainment ratio between two grids with 730×10^3 elements and 160×10^3 elements (Table 4). Consequently, a grid with 160K elements is chosen to conduct the calculation.

4.4 CFD Model Validation

The CFD model was validated using experimental results and with a fixed NXP equal to -29 mm. Because of the limitation of the experimental prototype, this NXP was the best available position for the ejector nozzle. The primary inlet condition is fixed in two different pressures (conditions II and III, Table 3), and the pressure at the secondary is varied to meet a fixed lift of 20°C. Figure 4(a) shows the experimental and numerical entrainment ratios for different ejector exit saturated temperatures. In this

figure, there is a good accordance between the results that confirms the validity of the CFD model prediction. In this diagram, a deviation between experimental and numerical results can be seen around the critical pressure. This phenomenon is also reported by (Mazzelli and Milazzo, 2015) who claimed that this deviation was due to wall roughness of the experimental ejector.

5. INFLUENCE OF NXP CHANGES ON THE FLOW PATTERN AND EJECTOR PERFORMANCE

The influence of the nozzle exit distance from the mixing chamber (NXP) is studied using a series of CFD simulations on the defined geometry in Table 2 and operating condition I (Table 3) for different ejector outlet pressures. NXP has been changed from -50 mm to -20 mm. Figure 4(b) shows the entrainment ratio versus ejector outlet pressure. As shown, with reducing the distance between the mixing chamber and the nozzle exit, the outlet critical pressure is increased. It should be noted that, when getting closer to the mixing chamber this variation in critical outlet pressure becomes relatively weak. For a NXP equal to -50mm, the pressure design-point is about 715Kpa compared to the case with NXP equal to -20mm, where the pressure design-point is equal to 770Kpa. This trend (increasing the critical pressure by moving the primary nozzle toward the mixing section) was also

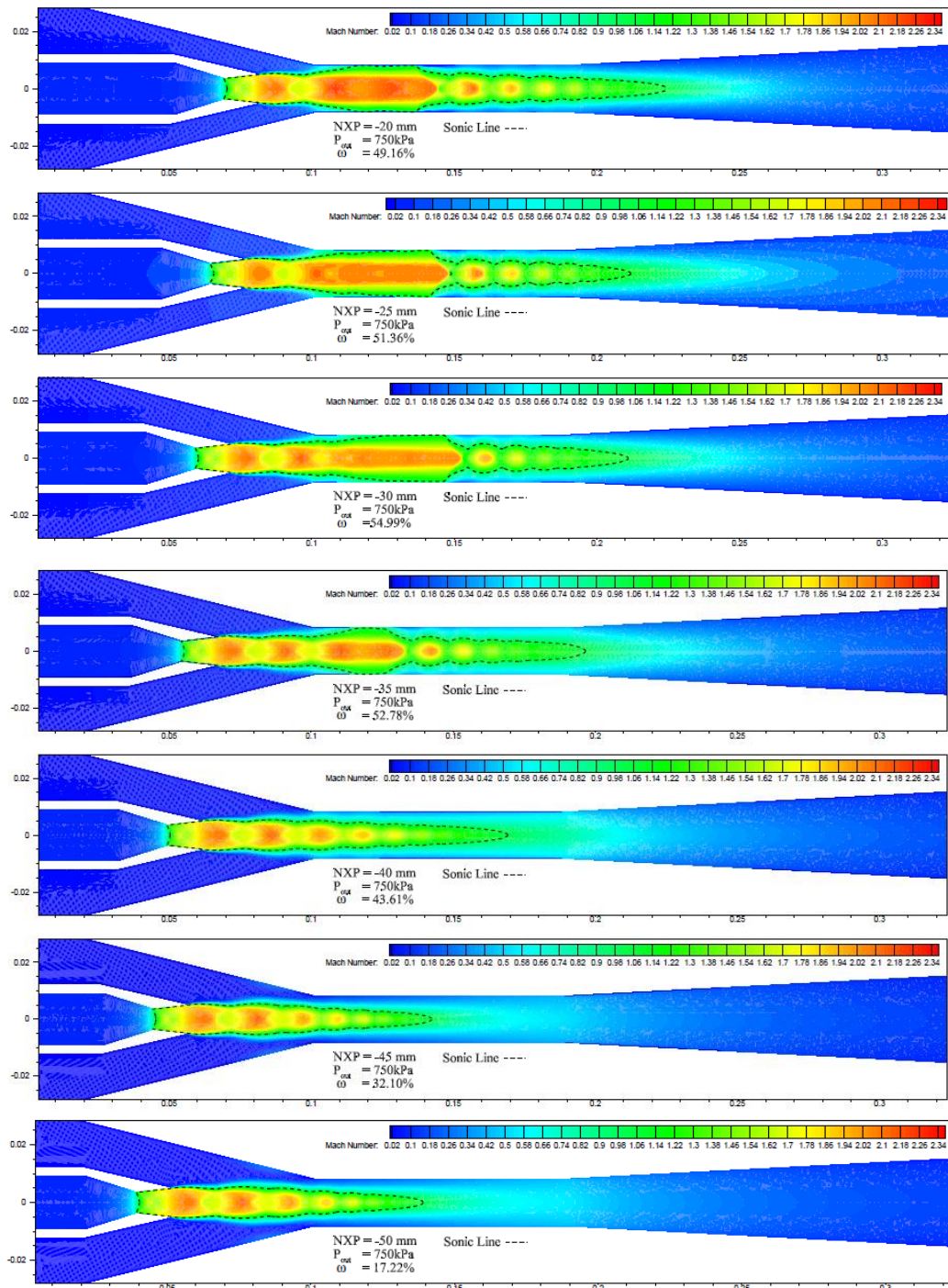


Fig. 5. Mach contours for seven different NXPs for working condition.

found with Aphornratana *et al.* (Aphornratana and Eames 1997) and Chunnanond *et al.* (Chunnanond and Aphornratana; 2004). However, Reddick *et al.* (Reddick, Sorin, Sapoundjiev and Aidoun; 2018) showed an opposite trend with their steam experimental test-bench. A numerical study of Varga *et al.* (Varga, Oliveira, and Diaconu, 2009) also showed the existence of an optimum value for critical pressure and NXP variation. Nonetheless, direct comparison is difficult due to different geometries of ejectors and considered operating conditions. Therefore, for any specific case, one

needs to have further investigation regarding this aspect of an ejector design. Fig. 4(b) shows that there is an optimum value for NXP where the highest entrainment ratio can be reached in a certain working condition (e.a. NXP = -30 mm). However, this optimum amount of NXP may not be unique and will change according to another operating condition. In this figure, the difference between the lowest and the highest entrainment ratio (0.49 and 0.55 respectively) is about 10%, which is significant. Mach contours for different NXPs and the operating condition #1 are drawn in Fig. 5. This figure reveals

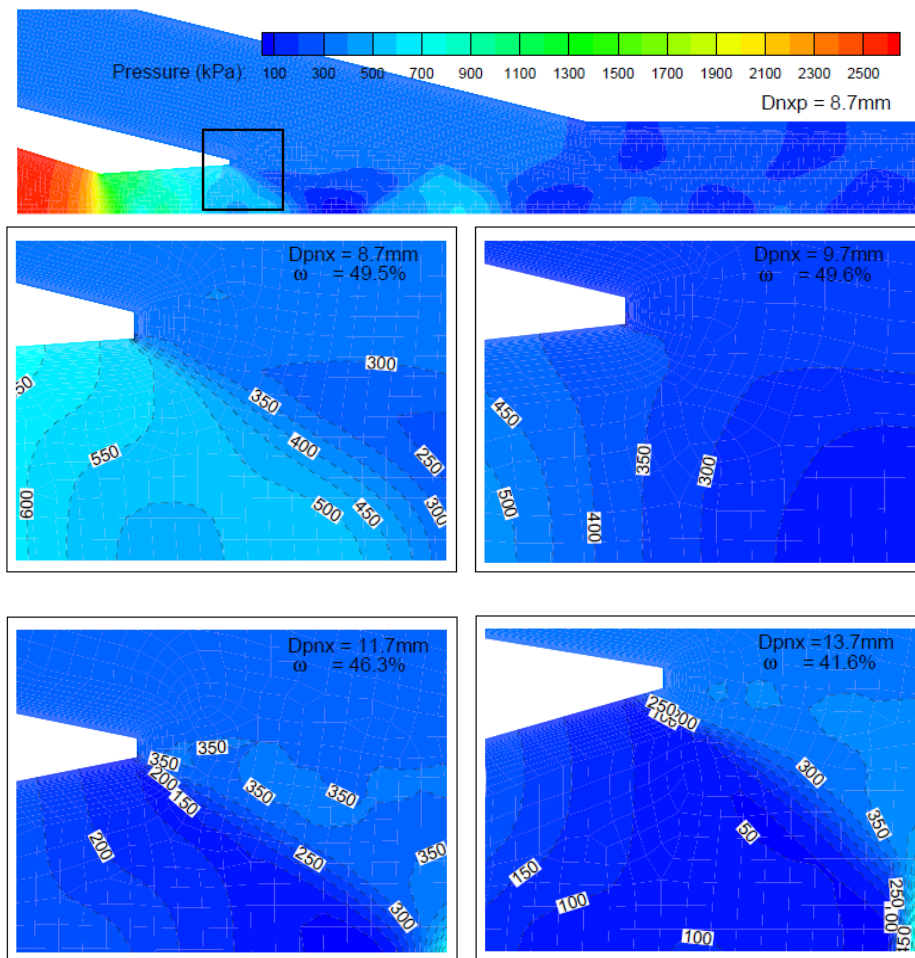


Fig. 6. Pressure contours at different nozzle exit diameters (NXP= - 30 mm).

the effect of NXP on the shocks occurring inside the ejector, and consequently the role that this element plays on ejector performance. In this figure, the separation between subsonic and supersonic areas is identified with sonic lines. As seen, for the NXPs for which the sonic line is attached to the ejector wall and the flow is double-choked, a higher entrainment ratio is obtained. This shows the importance of NXP in designing an ejector. This is also showing that with decreasing NXP and making the nozzle exit closer to the mixing chamber throat, the location of shocks are shifted further along the mixing chamber, which is the reason of having a higher critical outlet pressure. In general, for cases where the nozzle exit is too far from the mixing chamber (NXP is too large), the entrainment ratio starts to decrease because the primary flow is choked right away after the nozzle and, loses its energy to perform the suction of secondary flow. In contrast, for a case with a short NXP, secondary flow does not have enough area to exit and to interact with primary flow.

6. INFLUENCE OF THE NOZZLE EXIT DIAMETER ON FLOW CHARACTERISTICS

Dpnx is changed from 8.70mm to 13.70mm with an

increment of 1.0mm. For different Dpnxs, the length between the throat and the nozzle exit is fixed and the divergent angle (γ) is increased from 4° (Dpnx = 8.70 mm) to 16° (Dpnx = 13.70 mm). The change of nozzle exit can be defined based on the diameter Dpnx or the angle of the divergent part (γ) of the nozzle. However, for the sake of clarity and analysis purposes, the geometry and the results are reported based on Dpnx. Generally, in an ejector, the motive flow leaving the nozzle can be characterized in three different states; (1) over-expanded, where the motive pressure at the nozzle exit is lower than the secondary pressure, and flow could not expand more in the mixing area (shocks would consequently occur); (2) under-expanded, where the motive flow pressure at the nozzle exit is higher than the secondary flow pressure, the motive flow could expand more in the mixing area; and (3) in a condition where both nozzle exit pressure and secondary flow pressures are almost equal, which is the ideal condition for the motive flow exiting the nozzle (Chen, Dang, and Hihara; 2017). These three states have been demonstrated in Fig. 6, where all three under-expanded, ideally-expanded and over-expanded situations are shown for ejectors with Dpnx = 8.7mm, Dpnx=9.7mm and Dpnx=11.7mm, respectively. As seen, for Dpnx equal to 8.7mm the flow is under-expanded as the pressure right after the

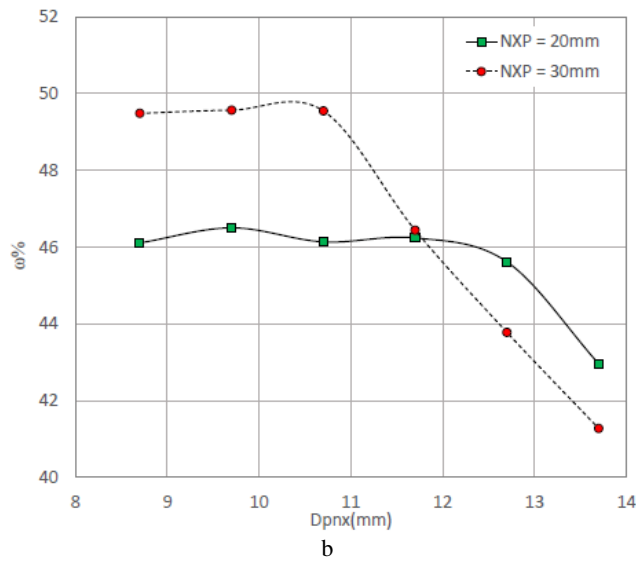
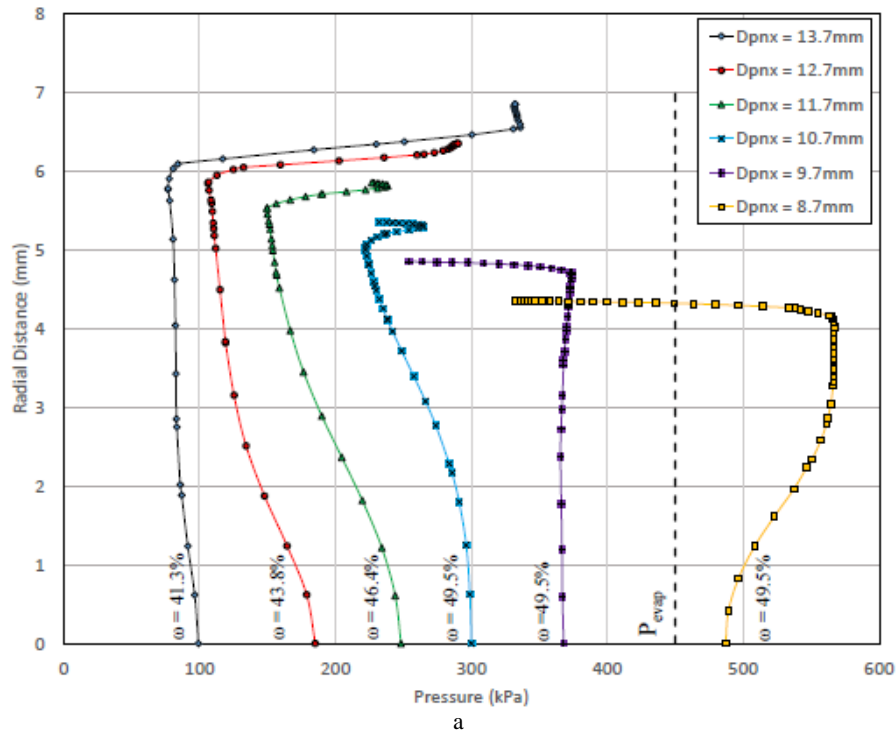


Fig. 7. (a) Pressure profiles at the nozzle exit for different diameters (b) Entrainment ratio versus nozzle exit diameter.

nozzle exit is close to 550kPa which is higher than the secondary pressure ($P_{evap} = 450\text{kPa}$). For D_{pnx} equal to 9.7mm the pressure at the exit of the nozzle is almost equal to the pressure at the secondary and the flow is ideally-expanded. For two other D_{pnx} s equal to 11.7mm and 13.7mm the pressure at the nozzle outlet is lower than the secondary pressure and the flow is so-called over-expanded. This has also been shown in Fig. 7(a), where the pressure profile at the exit of primary nozzle is shown. It can be implied from this figure that, with increasing the nozzle exit diameter, the exit pressure decreases. The secondary inlet pressure is also drawn in this figure.

Again, when comparing this figure and Fig. 6, it can be concluded that for those nozzles with a pressure profile closer to secondary inlet pressure, a higher entrainment ratio can be reached. Figure 8 shows the pressure profile along the x-axis of the ejector. As shown in this figure, for a nozzle exit diameter equal to 9.70mm, the amplitude of the pressure fluctuation are the lowest. This diagram along with Fig.6 implies that high pressure differences between the suction flow and the motive flow at the nozzle exit will amplify the chances of driving flow expansion, which is not necessarily useful for the functionality of an ejector, as shocks cause a sudden increase in

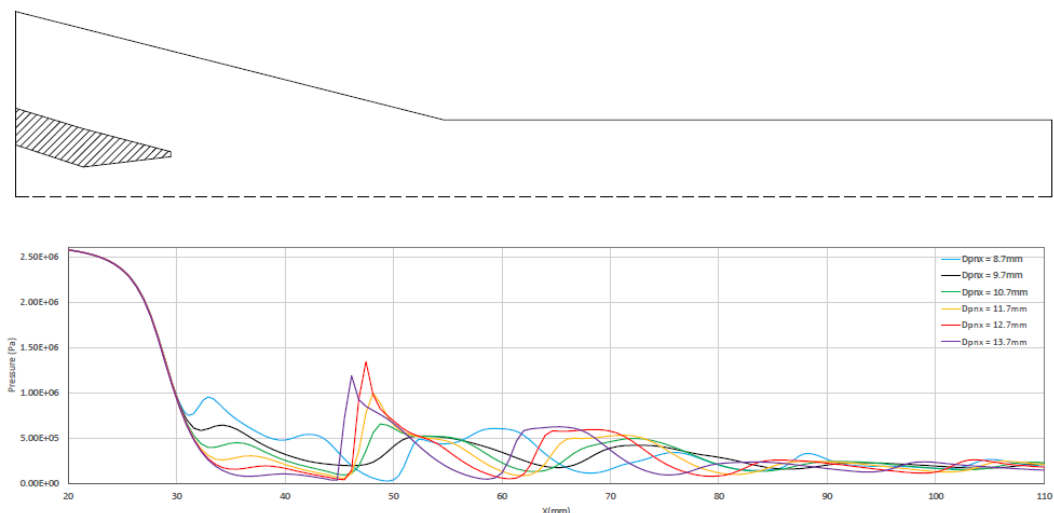


Fig. 8. Static pressure profile along the ejector X-axis for different nozzle exit throats (NXP=30mm).

pressure, temperature and entropy, consequently increasing irreversibility.

In general, from Fig. 6, Fig. 7(a) and Table 3 (the pressure at the secondary inlet for operating condition I), it can be concluded that the best diameter for the nozzle exit is where the flow pressure is equal to the secondary pressure. According to Fig.6, for the specified working condition and geometry, the best dimension for Dpnx should be between Dpnx = 8.7mm and Dpnx = 9.7mm. This is the state where the flow is ideally expanded at the nozzle exit. Figure 7(b) presents the entrainment ratio versus the nozzle exit diameter for two different NXPs. As shown in this figure, there is an optimum range for Dpnx to get the best entrainment ratio. Simulations were also carried out for a different NXP. The entrainment ratio drops significantly where the nozzle exit diameter is bigger than a critical value of the nozzle exit diameter. Based on the figure, this critical value for a NXP equal to 30mm is close to 10.7, and for a NXP equal to 20mm is 12.7mm. This shows that with different NXPs, the critical value of the nozzle exit diameter is changed. Although, based on Fig. 7(b), entrainment ratio is changed with NXP, however, as discussed in previous section, this impact is independent of Dpnx. This can also be observed from Fig.9 where the velocity contours are shown for two different NXPs and for different nozzle exits (Dpnx). According to this figure, although the flow structure is different for two NXPs, there are no significant changes to the flow structure right after the nozzle exit area. In order to investigate the relation between the nozzle exit diameter and the diameter of the mixing chamber (Dmix), the mixing chamber diameter was changed to two different sizes (one smaller and one bigger than the original size), and simulations were repeated for different nozzle exit sizes. The results show that as long as the drawn sonic line is attached to the wall of the mixing chamber and the flow is double choked (Fig.10), there is no significant relation between the mixing

chamber and nozzle exit diameters.

7. CONCLUSION

This study investigated numerical results of driving flow inside an ejector designed for a refrigeration cycle. At the first step, the effect of nozzle position with respect to the entrance of the mixing chamber was studied numerically. Simulations were carried out in order to determine an optimum value for NXP for a certain working condition. The results revealed that an optimum amount for NXP exists. However, this optimum value changes slightly from case to case according to different operating conditions. CFD simulations were also conducted in order to study the impact of nozzle shape changes on ejector performance. The results imply that appropriate expansion of the driving flow benefits the ejector functionality entrainment ratio standpoint. In other words, there is an optimum range of nozzle exit diameter where an ejector is at its highest state of performance. CFD simulation also showed that there is a condition for which the lowest fluctuation of pressure inside the ejector can be reached. These results imply that the over-expansion of the motive flow at the nozzle exit undermines ejector functionality. Hence, there is an optimum range of nozzle exit diameter for which the ejector performances are the highest. Finally, the simulations also indicated that for an ejector with different NXPs, the velocity distribution is different at the downstream.

REFERENCES

- Aphornratana, S. and I. W. Eames (1997). A small capacity steam-ejector refrigerator: experimental investigation of a system using ejector with movable primary nozzle. *International Journal of Refrigeration* 20(5), 352–358.

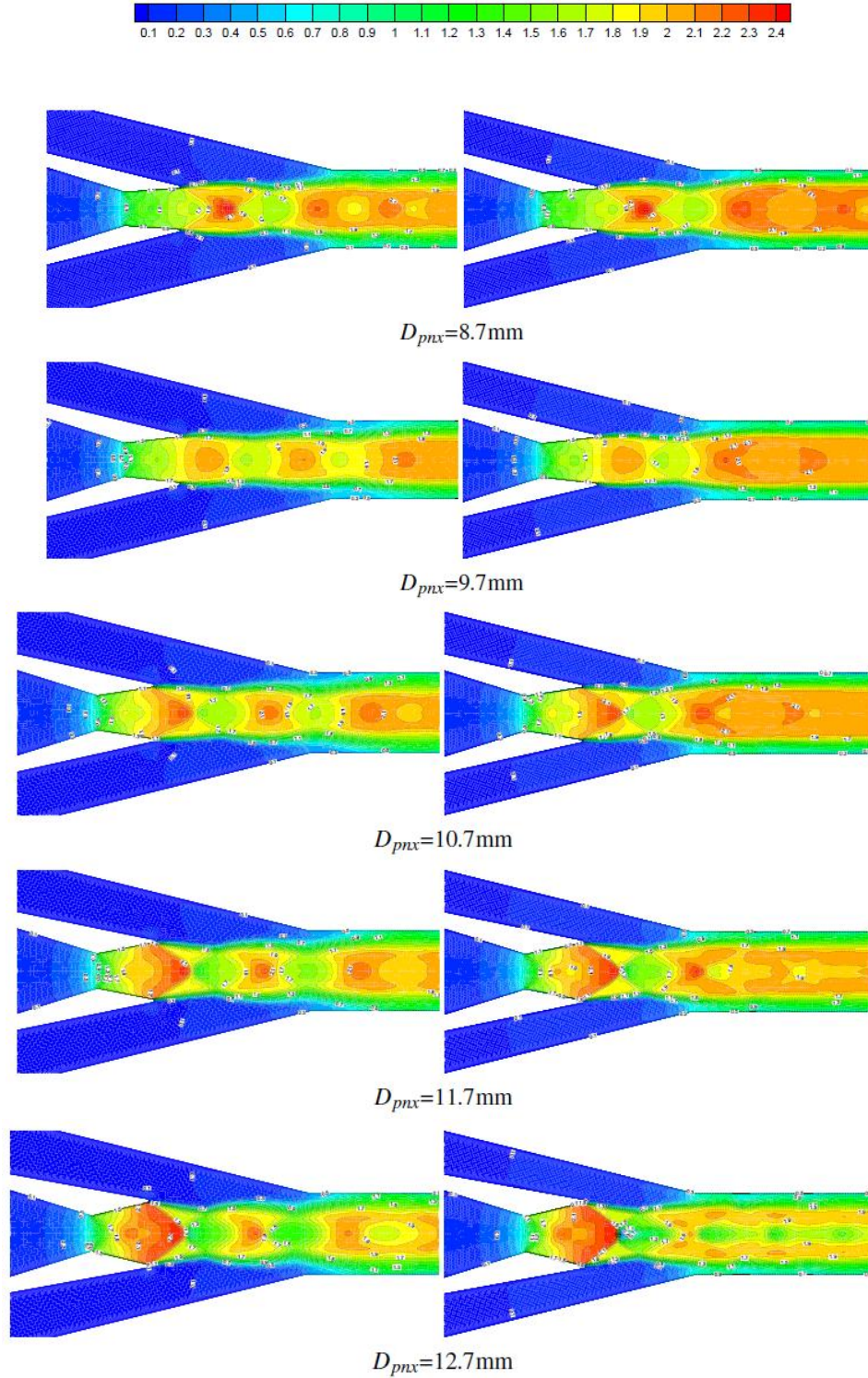


Fig. 9. Mach contours inside different ejectors for working condition I (left: NXP=30mm, right: NXP=20mm).

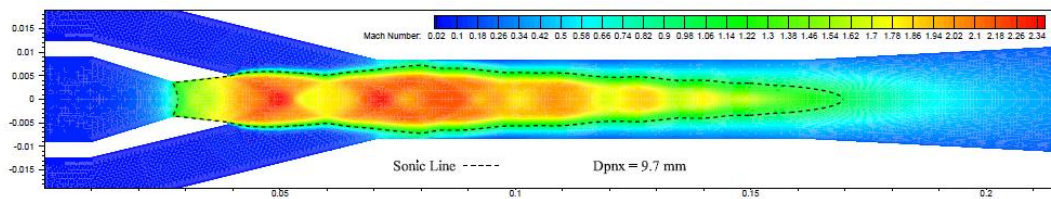


Fig. 10. Mach contour from CFD results for working condition I in Table 3 (NXP=30mm).

- Ariafar, K. (2012). Performance evaluation of a model thermocompressor using computational fluid dynamics. *International Journal of Mechanics* 6(1), 35–42.
- Bartosiewicz, Y., Z. Aidoun, P. Desevaux and Y. Mercadier (2005). Numerical and experimental investigations on supersonic ejectors. *International Journal of Heat and Fluid Flow* 26(1), 56–70.
- Boumaraf, L. and A. Lallemand (2005). Behavior of an ejector under nominal and non-nominal operating conditions. In *12th International Days of Thermique-JITH, T2*, 279–282.
- Chen, W., D. Chong, J. Yan and J. Liu (2013). The numerical analysis of the effect of geometrical factors on natural gas ejector performance. *Applied Thermal Engineering* 59(1-2), 21–29.
- Chen, Z., C. Dang and E. Hihara (2017). Investigations on driving flow expansion characteristics inside ejectors. *International Journal of Heat and Mass Transfer* 108, 490–500.
- Chong, D., M. Hu, W. Chen, J. Wang, J. Liu and J. Yan (2014). Experimental and numerical analysis of supersonic air ejector. *Applied Energy* 130, 679–684.
- Chunnanond, K. and S. Aphornratana (2004). An experimental investigation of a steam ejector refrigerator: the analysis of the pressure profile along the ejector. *Applied Thermal Engineering* 24(2-3), 311–322.
- Croquer, S., S. Poncet and Z. Aidoun (2016). Turbulence modeling of a single-phase r134a supersonic ejector. Part 1: Numerical benchmark. *International journal of refrigeration* 61, 140–152.
- Eames, I., S. Wu, M. Worall and S. Aphornratana (1999). An experimental investigation of steam ejectors for applications in jet-pump refrigerators powered by low-grade heat. *Proceedings of the Institution of Mechanical Engineers, Part A: Journal of Power and Energy* 213(5), 351–361.
- Falsafioon, M., Z. Aidoun and M. Poirier (2017). A numerical and experimental study of ejector internal flow structure and geometry modification for maximized performance. In *IOP Conference Series: Materials Science and Engineering* 280, 76–83. IOP Publishing.
- Huang, B., J. Chang, C. Wang and V. Petrenko (1999). A 1-d analysis of ejector performance. *International journal of refrigeration* 22(5), 354–364.
- Lemmon, E. W., M. L. Huber and M. O. McLinden (2002). Nist reference fluid thermodynamic and transport propertiesrefprop. *NIST standard reference database* 23, v7.
- Lin, C., W. Cai, Y. Li, J. Yan, Y. Hu and K. Giridharan (2013). Numerical investigation of geometry parameters for pressure recovery of an adjustable ejector in multi-evaporator refrigeration system. *Applied Thermal Engineering* 61(2), 649–656.
- Mazzelli, F. and A. Milazzo (2015). Performance analysis of a supersonic ejector cycle working with r245fa. *International journal of refrigeration* 49, 79–92.
- Menter, F. R. (1994). Two-equation eddy-viscosity turbulence models for engineering applications. *AIAA Journal* 32(8), 1598–1605.
- Nahdi, E., J. Champoussin, G. Hostache and J. Cheron (1993). Optimal geometric parameters of a cooling ejector-compressor. *International Journal of Refrigeration-Revue Internationale Du Froid* 16(1), 67–72.
- Pianthong, K., W. Seehanam, M. Behnia, T. Sriveerakul and S. Aphornratana (2007). Investigation and improvement of ejector refrigeration system using computational fluid dynamics technique. *Energy Conversion and Management* 48(9), 2556–2564.
- Reddick, C., M. Sorin, H. Sapoundjiev and Z. Aidoun (2018). Effect of a mixture of carbon dioxide and steam on ejector performance: An experimental parametric investigation. *Experimental Thermal and Fluid Science* 92, 353–365.
- Riffat, S. B. and S. Omer (2001). CFD modelling and experimental investigation of an ejector refrigeration system using methanol as the working fluid. *International Journal of Energy Research* 25(2), 115–128.
- Ruangtrakoon, N., T. Thongtip, S. Aphornratana and T. Sriveerakul (2013). CFD simulation on the effect of primary nozzle geometries for a steam ejector in refrigeration cycle. *International Journal of Thermal Sciences* 63, 133–145.
- Rusly, E., L. Aye, W. Charters and A. Ooi (2005). CFD analysis of ejector in a combined ejector cooling system. *International Journal of Refrigeration* 28(7), 1092–1101.
- Sriveerakul, T., S. Aphornratana and K. Chunnanond (2007a). Performance prediction of steam ejector using computational fluid dynamics: Part 1. validation of the CFD results. *International Journal of Thermal Sciences* 46(8), 812–822.
- Sriveerakul, T., S. Aphornratana and K. Chunnanond (2007b). Performance prediction of steam ejector using computational fluid dynamics: Part 2. flow structure of a steam ejector influenced by operating pressures and geometries. *International Journal of Thermal Sciences* 46(8), 823 – 833.
- Thongtip, T. and S. Aphornratana (2017). An experimental analysis of the impact of primary nozzle geometries on the ejector performance used in r141b ejector refrigerator. *Applied Thermal Engineering* 110, 89–101.
- Varga, S., A. C. Oliveira and B. Diaconu (2009).

- Influence of geometrical factors on steam ejector performance—a numerical assessment. *International journal of refrigeration* 32(7), 1694–1701.
- Wang, L., J. Yan, C. Wang and X. Li (2017). Numerical study on optimization of ejector primary nozzle geometries. *International Journal of Refrigeration* 76, 219–229.
- Watanawanavet, S. (2008). *CFD optimization study of high-efficiency jet ejectors*. Ph. D. thesis, Texas A&M University.
- Yan, J., C. Lin, W. Cai, H. Chen and H. Wang (2016). Experimental study on key geometric parameters of an r134a ejector cooling system. *International journal of refrigeration* 67, 102–108.
- Yan, J., W. Cai, C. Lin, C. Li and Y. Li (2016). Experimental study on performance of a hybrid ejector-vapor compression cycle. *Energy Conversion and Management* 113, 36–43.
- Yapıcı, R. (2008). Experimental investigation of performance of vapor ejector refrigeration system using refrigerant r123. *Energy Conversion and Management* 49(5), 953–961.
- Zhu, Y., W. Cai, C. Wen and Y. Li (2009). Numerical investigation of geometry parameters for design of high performance ejectors. *Applied Thermal Engineering* 29(5), 898–905.